Available online at www.sciencedirect.com
SCIENCE DIRECT
Polymer 46 (2005) 10466–10477
polymer
www.elsevier.com/locate/polymer

Anisotropic microstructure-impact fracture behavior relationship of polycarbonate/polyethylene blends injection-molded at different temperatures

Zhong-Ming Li*, Zhi-Qi Qian, Ming-Bo Yang, Wei Yang, Bang-Hu Xie, Rui Huang

State Key Laboratory of Polymer Materials Engineering, College of Polymer Science and Engineering, Sichuan University, Chengdu, Sichuan 610065, People's Republic of China

Received 5 January 2005; received in revised form 20 July 2005; accepted 26 August 2005
Available online 21 September 2005

Abstract

Polycarbonate (PC)/polyethylene (PE) blend was injection molded at three temperatures: 190, 230 and 275 °C. Due to different deformability of PC phase at the different molding temperatures, the blends exhibit different morphologies. The sample molded at 190 °C only contained many uniformly dispersed spherical PC particles due to the incapability of flow and deformation of PC phase at this temperature. The samples molded at both 230 and 275 °C showed typical anisotropic (skin–core) structures, and there were many injection-induced PC fibers in the sub-skin layer. The DSC measurement showed that higher molding temperature leads to higher crystallinity and more perfect crystals of PE phase. The impact fracture of three bars behaves differently in the following aspects: (1) overall fracture surface, (2) craze and micro-void formation (stress whitening), (3) fibrillation of PE, and (4) plastic deformation of PC dispersed phase. As the molding temperature increases, the stress whitening becomes stronger, the shear lips become thicker, the amount of the stick–slip lines and the micro-voids increases, and the voids become smaller. Moreover, upon impact fracturing, numerous fibrils of PE were formed in 230- and 275-bars, at the same time, obvious plastic deformation of PC fibers occurred in the 275-bar. All these microscopic features demonstrate the impact toughness increases with molding temperature. Lamellae texture evolution and high interfacial contact were employed to partially interpret the impact fracture behavior. Numerous filaments generated around PC particles on the fracture surfaces, which bridged the PC particles and PE matrix, indicated a high interfacial adhesion between PC particles and PE matrix.

Keywords: Polycarbonate (PC)/polyethylene (PE) blend; Injection molding; Impact fracture behavior

1. Introduction

Strength and toughness of polymer materials are two of the most important properties for specific applications. Efforts have been made to improve these two properties [1–3]. Numerous investigations reveal that the toughness of polymers and their blends is related to the aggregate structure and phase morphology generated in situ during melt processing [4,5]. Wu is the first researcher to quantitatively evaluate the correlation between toughness and dispersed phase size of polymer blends [6,7]. It is proposed that the critical matrix ligament thickness (T_c) is the only parameter to determine the brittle–ductile transition of the blends. Only when the matrix ligament thickness (T) is smaller than T_c that the shear yielding of matrix ligament and the brittle–ductile transition can take place. For a given blend, T_c is independent of the volume fraction and particle size of the rubber phase. If the neighboring particles are taken into account, the stress fields around individual particles are expected to interfere or overlap with each other and hence more massive shear yielding is expected to pervade the matrix as T is decreased. Wu's theory is quite effective in rubber toughened polymer systems [8], and also applicable in some organic rigid filler filled polymer composites [9]. However, it cannot predict the fracture behavior of many immiscible blends composed of two or more structurally different thermoplastics.

Injection molding, as one of the most complicated polymer processing techniques, imparts high stress and rapid cooling as the polymers are formed into useful shapes [10]. For immiscible polymer blends, under both strong stress field and non-isothermal temperature profile, the deformable minor phase can be deformed in situ into a variety of morphological

* Corresponding author. Fax: +86 28 8540 5324.
E-mail address: zm_li@263.net.cn (Z.-M. Li).

0032-3861/$ - see front matter © 2005 Elsevier Ltd. All rights reserved.
doi:10.1016/j.polymer.2005.08.081

structures such as spheres, ellipsoids, fibers, and plates [11–14]. Additionally, the microstructure is unevenly distributed in the injection-molded parts, displaying an anisotropic skin–core morphology [15–20]. This leads to more difficulty in revealing the influences of the morphology on the mechanical properties of the injection-molded blends. Karger-Kocsis found that during injection molding, a skin–core morphology was formed in both the continuous polypropylene (PP) matrix and the modified PP blends containing rubber particles deformed to different degrees [4]. The failure during tensile testing and impact loading is initiated in the shear zone along the skin–core boundary. The final failure mode depends on the interaction of crazing and shear yielding. Recently, Karger-Kocsis and Mouzakis [21] studied the effect of injection molding induced skin–core morphology on the behavior of rubber-toughened polypropylene (RTPP) system by the essential work of facture (EWF) method. RTPP with high content of ethylene/propylene rubber (EPR) showed no skin–core structure and the EWF approach worked well in this case. However the EWF approach failed in the case of RTPP with low content of EPR. RTPP with low content of EPR exhibited pronounced skin–core morphology. This morphology caused necking instead of crack propagation in deeply double edge-notched specimens under tensile loading along the mold filling direction. The necking process was accompanied by a large scattering and yielded highly unrealistic specific essential work of fracture values. Fu et al. utilized dynamic packing injection molding to control the size and shape of ethylene–propylene–diene monomer elastomer (EPDM) in PP, and obtained spherical and elongated oriented EPDM particles in the blends [22]. It was observed that the impact fracture direction with respect to the orientation direction plays an important role in determining the impact strength of the blends [23]. Wu's theory holds true as long as the rubber particles are roughly spherical, but no longer valid for the blends containing elongated and oriented rubber particles whose long axes are perpendicular to or oblique with the crack growth direction [22,23].

In our previous studies [24–26], the injection induced morphology and its influences on the tensile behavior of polycarbonate (PC)/polyethylene (PE) blends were thoroughly investigated. The main conclusions are: (1) The shape and size of the dispersed PC phase depended on the injection molding parameters such as injection speed and temperature as well as the positions in the bar. When the injection temperature is high enough to melt PC and PE (e.g. 275 °C), the blend exhibits a typical skin–core structure including four layers: surface, sub-skin, intermediate layers and core zone [23]. Among the four layers, the sub-skin layer, where a great amount of PC fibers are generated, is the thickest and became thinner gradually along the melt flow direction. Moreover, the dispersed phase became smaller from the gate end toward the non-gate end. In contrast, when the injection temperature (e.g. 190 °C) is below a critical value PE is melted while PC stays in solid state. The injection-molded PC/PE blend assumes a homogeneous morphology where the PC particles are uniformly dispersed in PE matrix. In this case, the high speed filling flow has little influence on the formation and distribution of PC dispersed particles [26]. (2) The blend molded at high temperatures exhibited unusual double tensile yielding [24]. While the blend molded at low temperatures showed smaller PC reinforcement on PE. And the blend does not have double yielding, and exhibits a stress–strain behavior as a common immiscible blend. It was suggested that the double yielding was morphology dependent [26]. The first yielding was that of PE matrix and the second one was of PC fibers. Moreover, it is the frictional force in the interfaces between PC and PE that transferred the stress to the PC fibers, hence giving rise to the reinforcement of PE by PC.

These findings arouse our curiosity to further explore the relationship between the injection induced skin–core morphology and the impact fracture behavior of PC/PE blends. In the open literature, the comparison between the injection-molded bars with anisotropic and homogeneous phase morphologies has not been made, partly due to the fact that these two phase structures are not simultaneously available with traditional injection processing parameters. In this study, a wide injection temperature range (190, 230 and 275 °C, respectively) was used to prepare the PC/PE samples with different morphologies including skin–core and homogeneous structures. The impact fracture behavior of these samples was examined to further reveal the anisotropic morphology–property relationship in injection-molded PC/PE blends.

2. Experimental

2.1. Materials

The resins used were high density PE and PC, where PC was the dispersed phase and PE the matrix. PE (Model 5000S) with number average molecular weight $\bar{M}_n$ of 5.28×10^5 g/mol was obtained from DaQing Petroleum Chemical Co., China. Its melt flow rate (MFR) is 0.9 g/10 min at 190 °C. PC (Model K1300) was obtained from Teijin Chemical Co. Ltd, Hiroshima, Japan. Its $\bar{M}_n$ approximately $2.8–3.2\times10^4$ g/mol with a molecular weight distribution index of 2.1 by GPC.

2.2. Sample preparation

PC was dried for 12 h under vacuum at 100 °C before processing to avoid hydrolytic degradation. The dried PC pellets were dry-mixed with PE pellets with a fixed weight ratio of 15/85. The mixture was then blended in a twin-screw extruder with a temperature profile of 190, 230, 250, 265, 275 and 280 °C from hopper to die. The screw speed was maintained at 120 rpm. The extruded thread was pelletized and dried before injection molding. Rectangular bars were molded by an injection molding machine made in Nissan, Japan. The mold used had two-cavities and a single gate in each cavity, which assured no weldline in the bars. The schematic representation of the bar is shown in Fig. 1. Injection molding parameters were: injection speed: 10.0 mm/s; injection flow rate: 3.23 cm^3/s; total cycle time: 55.0 s; injection time: 5.5 s; holding pressure time: 12 s; cooling time: 40 s; injection pressure: 80 MPa; hold pressure: 40 MPa; back pressure: 40 MPa; screw speed: 100 rpm; mold

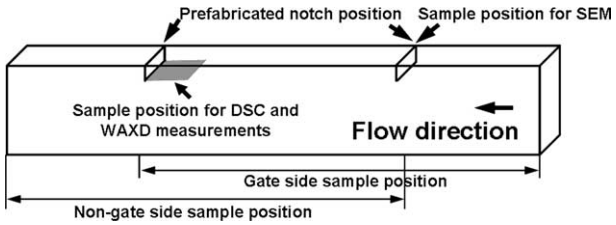

Fig. 1. Schematic representation of the sites where samples for Notch impact test, DSC, WAXD and SEM were taken.

temperature: 40 °C. Three temperature profiles used were: 170, 190, 190, 190 °C; 170, 190, 230, 230 °C; and 240, 265, 275, 270 °C from feed zone to nozzle. For the sake of brevity, hereafter, these injection temperature profiles are, respectively, referred to as 190, 230 and 275 °C. The corresponding bars are named 190-, 230-, and 275-bar.

2.3. Impact strength testing

The standard single-edge notched specimens (4 mm × 10 mm × 80 mm) for Izod impact tests were cut from the injection-molded rectangular bars. The positions, where the specimens were cut, were, respectively, chosen close to the gate side and the non-gate side. Two groups of samples were obtained as shown in Fig. 1. The measurements were performed with an I200XJU-2.75 Impact tester according to ISO 179 at 25 °C. Five specimens were tested and their average value was reported.

2.4. Differential scanning calorimetry (DSC) measurement

Thermal analysis was performed with a heating rate of 10 °C/min using a Netzsch DSC 204 differential scanning calorimeter. The samples for DSC tests were taken from the sub-skin layer of the blend parallel to the flow direction as shown in Fig. 1. Particular care was taken to protect the sample from any plastic deformation, which may affect the crystal features. The peak temperature of melting was taken as the melting temperature T_m. The crystallinity of PE in the blends was calculated by:

$$X_c = \frac{\Delta H}{\phi \Delta H_0} \quad (1)$$

where $\Delta H_0 = 290$ J/g [27] was the heat of fusion for a 100% crystalline PE, ΔH was the measured heat of fusion for PE in the blends, ϕ is the weight fraction of PE in the blends, 0.85 in this study.

2.5. Wide-angle X-ray diffraction (WAXD) measurement

A Philips X'Pert Graphics & Identify was used to measure the wide angle X-ray diffraction (WAXD) spectra at 35 kV and 25 mA, using Ni-filtered radiation. The monochromated X-ray from Cu K_α radiation of 0.154 nm was used and the reflection mode was used. The scanning 2θ range is from 10 to 35° with a scanning rate of 5 °/min. A thin sheet of sample whose plane is parallel to the flow direction is used (Fig. 1).

2.6. Scanning electron microscopy (SEM) observation

The phase morphology was characterized with a JEOL JSM-5900LV scanning electron microscope. The samples were frozen in liquid nitrogen for 1 h then impact fractured for SEM analysis. The position of the fracture close to the non-gate end of the specimens was fixed by the prefabricated flat crack in one side perpendicular to the melt flow direction (Fig. 1). The freshly fractured surface was gold sputtered before SEM analysis.

3. Results and discussion

Fig. 2(a)–(c) presents the morphology from the surface towards the center of the bars obtained at three injection temperatures 190, 230 and 275 °C, respectively. When molded at 230 and 275 °C, a gradient morphology (skin–core structure) was formed as in most injection-molded incompatible blends [4,15]. The sample molded at 190 °C shows a relatively homogeneous morphology where most PC particles are uniformly dispersed with a thin matrix layer near the surface of the sample. The size of the PC domains in the 230- and 275-bars is obviously smaller than that in the 190-bar, indicating different degree of plastic deformation at various molding temperatures. Moreover, the PC particles in the 190-bar appear in the form of spherical particles, while those in the 230- and 275-bars show highly elongated orientation in some regions. The flow temperature of PC is about 230 °C, below which the PC particles are hard to deform [26]. Thus, the dispersed PC particles observed in Fig. 2(a) are generated during twin-screw extrusion [28]. The detailed description of the morphology of injection-molded PC/PE blends under different processing parameters was reported elsewhere [24–26]. Fig. 3 shows the morphology of the core layer of the blend molded at 275 °C. The dispersed PC phase is mostly spherical as observed in the common injection-molded incompartible blends, with some ellipsoidal and rodlike particles. A schematic representation of the morphology of PC/PE blends injection-molded at high and low temperatures [24–26] is shown in Fig. 4(a) and (b), respectively. There are four layers (surface, sub-skin, intermediate layer and core zone) for the blend molded at high temperature (Fig. 4(a)) while the phase structure for the blend molded at 190 °C is almost uniform (Fig. 4(b)) where the particles are mostly spherical except a thin surface layer where nearly no PC particles was observed. The mechanism for the formation of different structures was discussed elsewhere [23,25].

Table 1 shows the notch impact strength of the injection-molded PC/PE bars obtained at different temperatures. The gate side and the non-gate side of the bars have different impact toughness and they are listed in Table 1. The 275-bars were not fractured by the impact testing (Fig. 5). Thus, its data are only for comparison. The 275-bar showed highest impact strength while the 190-bar showed the lowest strength. This implies that

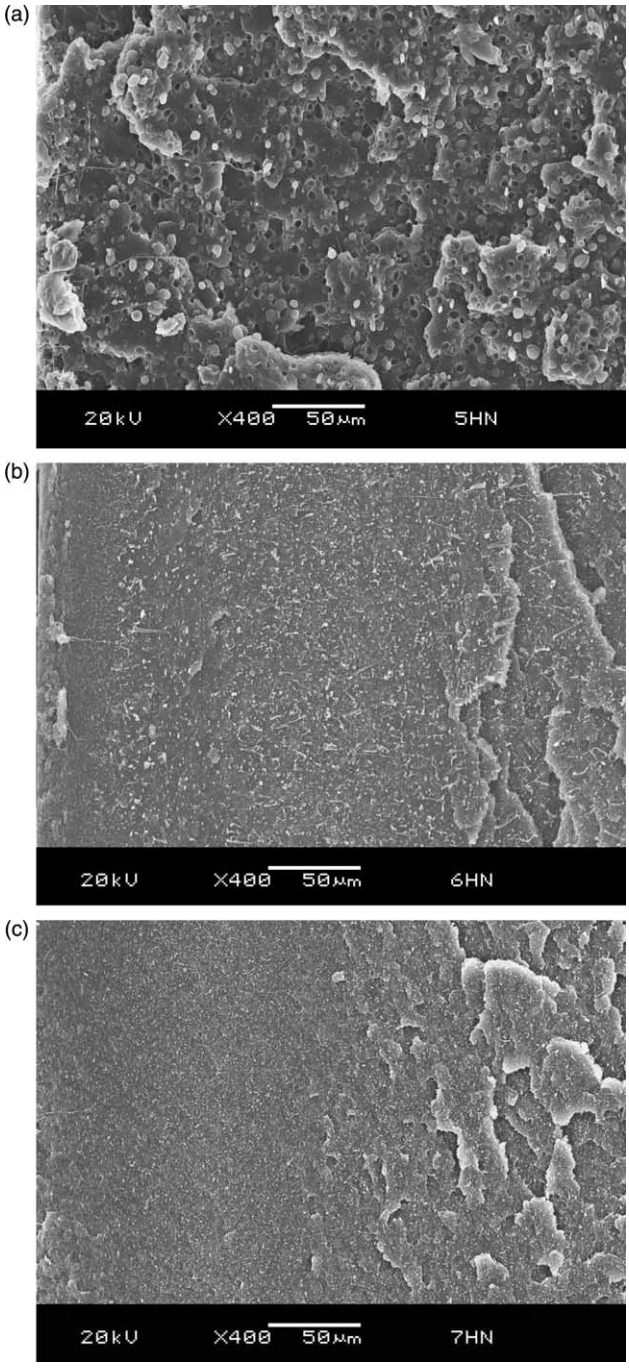

Fig. 2. SEM micrographs of the injection-molded PC/PE samples at non-gate side. Injection temperature: (a) 190 °C; (b) 230 °C; (c) 275 °C. Left to right corresponds to the surface to the center of the samples.

the impact toughness of injection-molded PC/PE blend is morphology dependent and is mainly determined by processing parameters. Additionally, the gate side constantly has higher toughness than the non-gate side, indicating that the toughness of the specimens has position dependency [23].

It is well known that during injection molding there are complex stress and temperature fields in which the polymers, especially the crystalline ones, may a have great change in aggregate structures and phase morphology. To interpret the fracture behavior, DSC, WAXD, and SEM were employed to

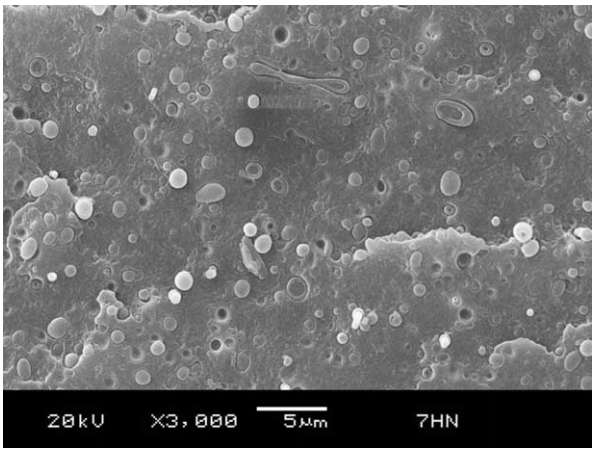

Fig. 3. SEM micrograph of the core zone near the non-gate side for the 275-bar.

investigate the crystallization behavior, crystal structure and phase morphology of the injection-molded PC/PE blends.

Fig. 6(a) presents the DSC heating curves of different samples at a rate of 10 °C/min. Since the greatest structure change occurred in the sub-skin layer [29], the samples for DSC tests were taken from the sub-skin layer of the blends parallel to the flow direction as shown in Fig. 1. The melting temperature and crystallinity of PE phase obtained from DSC testing are listed in Table 2. It is found that the bars molded at 230 and 275 °C show higher melting temperature than that at 190 °C and the crystallinity of PE phase increases with molding temperature. These might be caused by the different cooling rates during molding. Generally lower molding temperature means faster cooling and less duration for crystallization thus, leads to less perfect crystal and lower crystallinity. In addition, PC fibers generated at high temperatures may act as effective heterogeneous nucleating agent for PE [30,31]. This might be

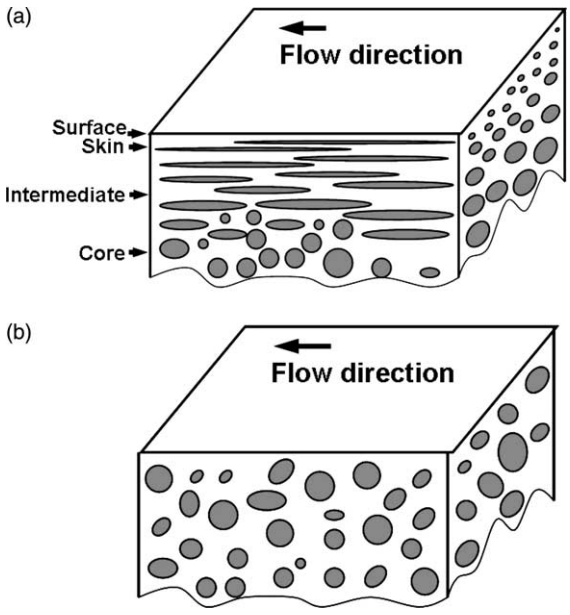

Fig. 4. The schematic representation for the morphology of the injection-molded PC/PE blend bars at different temperatures. (a) high temperature (e g. 230 and 275 °C), (b) low temperature (e.g. 190 °C).

Table 1
The notched impact strength of the samples injection-molded at 190, 230 and 275 °C

Injection molding temperature (°C)	Notched impact strength (kJ/m^2)	
	Gate side	Non-gate side
190	8.8±0.3	7.3±0.2
230	15.8±0.5	11.7±0.4
275	20.9±0.3	18.2±0.2[a]

[a] The samples were not impact broken.

another reason for higher crystallinity of PE for the blends molded at higher temperature.

Interestingly, there is a shoulder melting peak at the high temperature side of the main melting peak in the DCS curves of the blends molded at 230 and 190 °C. And the one for 230 °C is less pronounced than the one for 190 °C. While the blend at 275 °C shows only one main melting peak. The reason might be as follows. There exists high shear and elongational field during mold filling especially for the melt in contact with the solidified layer, which causes stretching and alignment of polymer molecules along flow direction. When polymers crystallize from an oriented or strained melt, shish kebab texture is usually a predominant feature of their crystal morphology [32–34]. High shearing field assists in the formation of nuclei by the alignment of polymer chains in the supercooled melt along the shear direction. This alignment may act as a precursor for the formation of stable primary nuclei. Many nuclei of tens of angstroms can rapidly grow and forge connectivity along the flow direction to imprint the stress field [35–37]. Moreover, the stability of the orientation-induced structures formed due to the shear fields depends on the relaxations of the polymer chains in the melt. The relaxation primarily depends on temperature and chain length (molecular weight). Only one melting peak was observed for the sample molded at 275 °C, implying that only one crystal structure (most likely a spherulite) exists. While there are two melting peaks observed for the 190 and 230 °C molded samples, indicating that there are two crystal structures existing, supposedly, the so-called shish kebab and spherulite. The peak at lower temperature might be the melting of spherulites or kebab, whereas that at higher temperature might

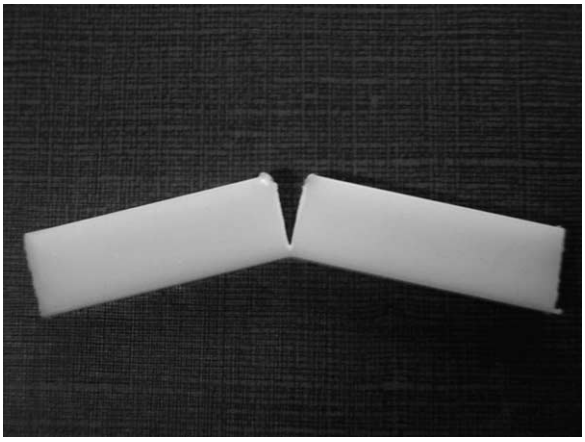

Fig. 5. Impact fractured 275-bar.

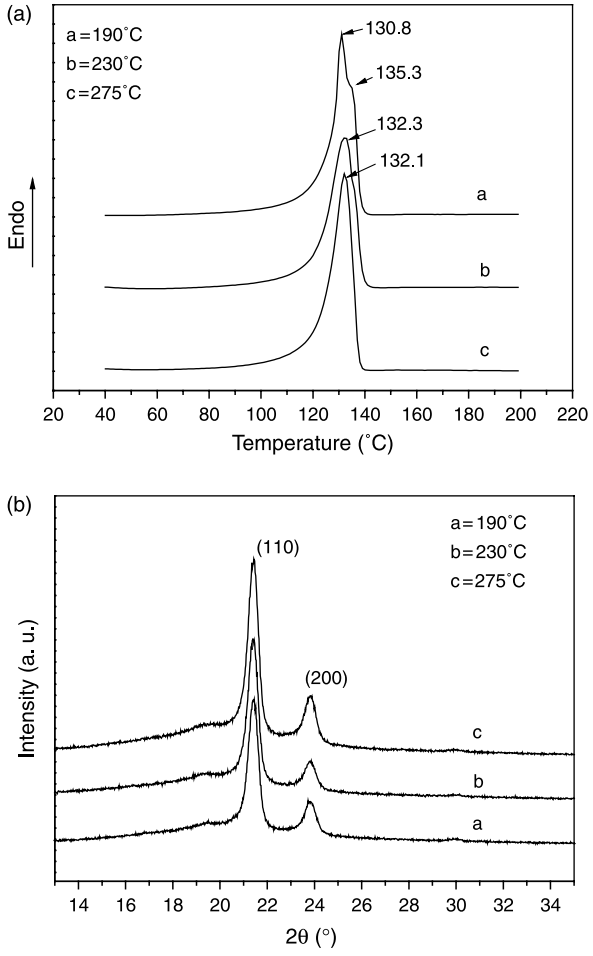

Fig. 6. DSC and WAXD curves for injection-molded PC/PE blends. (a) DSC; (b) WAXD

be the melting of the stretched chain of shish kebab [38,39]. When molded at 275 °C, the oriented PE molecules formed during mold filling experienced enough relaxation. Subsequent crystallite growth took place on the disordered nuclei (homo- and heterogeneous nucleating) from the coiling chains. At lower injection temperatures, the orientation of PE molecules was partially reserved. Thus, the shish kebab structure might be formed. As a result, the sample molded at 190 °C shows a more pronounced melting peak of shish crystals than that molded at 230 °C.

Fig. 6(b) shows the WAXD curves for three different temperature molded bars. Except the intensities of the peaks, all the WAXD scans reveal identical reflections to those for neat PE. Three peaks located at 2θ positions of 19.41, 21.54, and 23.84° are observed. The most intense peaks are located

Table 2
The melting temperature and crystallinity of PE in the injection-molded PC/PE blends obtained from DSC analysis

	Injection molding temperature (°C)		
	190	230	275
Melting temperature (°C)	130.8	132.3	132.1
Melting enthalpy (J/g)	136.0	144.2	150.0
Crystallinity (%)	56.0	59.3	61.7

at 21.54 and 23.84° and correspond to the 110 and 200 reflections in an orthorhombic form of PE, respectively. This means that there is no difference in crystal forms among three samples [40].

Fig. 7(a)–(c) present the low-magnification SEM fractographs of impact fractured PC/PE blends molded at 190, 230 and 275 °C, respectively. Apparently, the facture surfaces are composed of three distinct zones: slow crack-growth zone (around A), rapid crack-growth zone (around B) with small shear lips (S) close to both surfaces of the bar, and crack blunting zone (around C). For simplicity these three zones will be referred to as A, B and C zones, respectively, hereafter. The 275-bar was not completely fractured by impact (Fig. 5). Zone D was made by cutting with a razor, which is reasonably assigned to the crack blunting zone (Zone C).

Zone A is a small zone associated with fracture initiation, and was formed during the period when impact load rose to its peak value [41]. There is no obvious difference among Zone As for the three bars except that the 275-bar showed the most remarkable stress whitening as shown in Fig. 7(c), which implies that injection generated PC fibers facilitate craze and micro-void formation in the PE matrix, and cavitation between dispersed PC phase and PE matrix. The 230-bar also contains some PC fibers, but the sub-skin layer where the PC fibers are localized is thinner. The depth of the prefabricated crack for impact testing is approximately equal to the thickness of surface and sub-skin layers. Zone A of the 230- bar is located in the intermediate layer where PC spherical and fibrillar particles coexist as shown in Fig. 9(a). Therefore, the 230-bar showed less stress whitening.

The breakdown of the craze initiation might lead to the propagation of a crack (Zone B). Zone B itself is usually characterized by hackle zone, interior zone and shear lip. The sudden burst of energy when the slow crack-growth zone breaks down drives the crack to advance at a faster rate. At such a high speed, the material does not have enough time to relax, resulting in brittle-like fracture, leaving the hackle structure on the fracture surface [41]. However, Zone Bs in

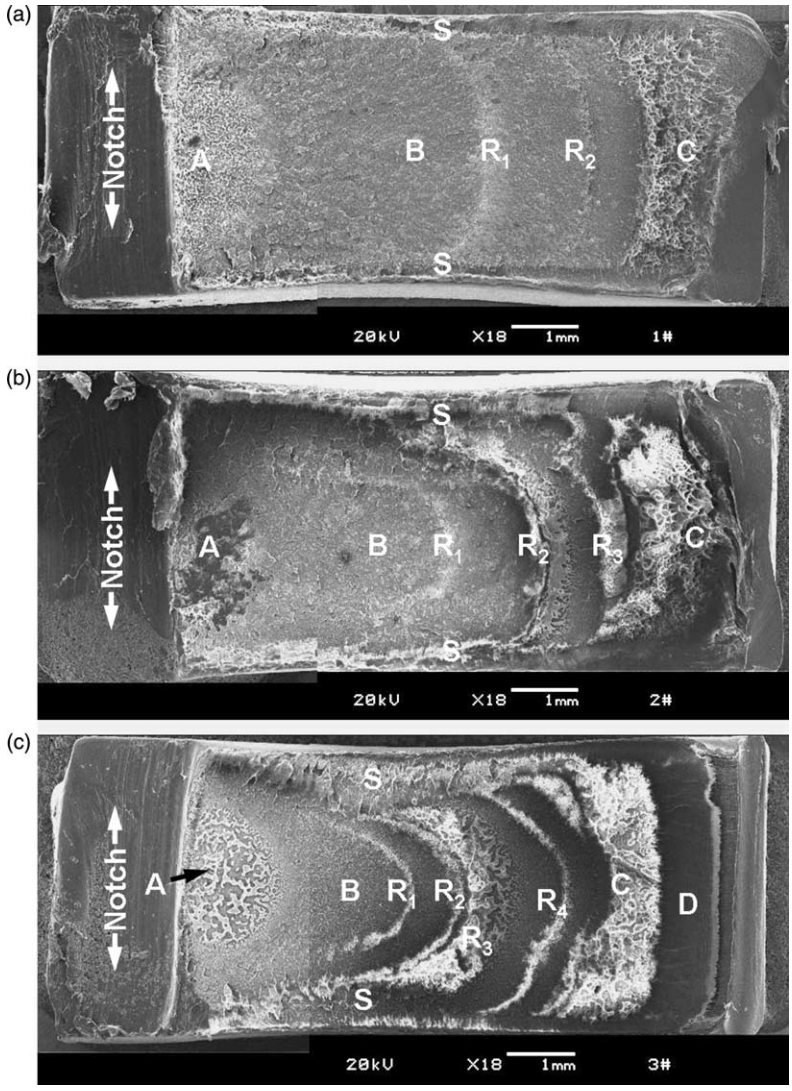

Fig. 7. Low magnification SEM micrographs of impact fractured surfaces. (a) 190 °C; (b) 230 °C; (c) 275 °C. The capital letters in the pictures, A, fracture initiation region (low crack-growth region); B, rapid crack-growth region; C, crack blunting region; S, shear lip; R, stick–slip line.

Fig. 9 show absence of the hackle structures. The following features were observed for Zone B of the three samples:

(1) They all show fast stick–slip like crack propagation [42]. The occurrence of the stick–slip lines is characterized by the protuberant ridges. The number of the ridges is different. There are four ridges in Zone B of 275-bar (R1–R4), three ridges for 230-bar (R1–R3), and only two (R1 and R2) for the 190-bar. These ridges reflected the resistance to crack growth. The crack must have been temporarily slowed at these stick–lip lines [41]. Moreover, the observation of Fig. 7 indicates that the formation of stick–slip line is also related to the blend morphology. Generally, more fibers and thicker fiber-contained layer shall result in larger ridges.
(2) The stress whitening in the protuberant ridges indicates large plastic deformation upon impact. This is also evidence of fracture speed decreasing in the stick–slip line. The 275-bar showed the strongest whitening as its Zone A. The whitening of 230- and 275-bars became more pronounced while further away from the notch (from R1 to R4), while the ridges of 190-bar showed almost same degree of whitening on the fracture surface. This also demonstrates the influence of injection-molded PC fibers on the stress whitening. There are nearly no PC fibers in the 190-bar, so the whitening is the weakest and no difference between R1 and R2. For the 230-bar, with R1 in the core zone, R2 in the intermediate layer, and R3 in the sub-skin layer, their stress whitening becomes stronger and stronger from R1 to R3 partly due to the difference of their PC phase shape. The case of 275-bar is similar to the 230-bar except an additional R4 ridge and larger area of each ridge, especially R3.
(3) For all these three bars, there are shear lips (S, as shown in Fig. 7) around Zone Bs. These are regions that underwent somewhat ductile deformation as a result of the biaxial stress field present at the free surface of the specimen [41]. But the thickness of the shear lips is different. Generally, the thickness increases along with the fracture direction. The 275-bar showed thickest shear lips, while the 190-bar the thinnest. These might also be a result of different amount of PC fibers inside the zones. More fibers resulted in thicker shear lips.

The crack blunting region (Zone C) is at the end of the fracture surface. Strictly speaking this region is part of the shear lips but with distinct features. The rather irregular crack blunting region and strong stress whitening implied large plastic deformation. The area of Zone C and the intensity of the whitening increased with the increase of the injection temperature. Roughly, the area of Zone C and D is three times and 1.5 times larger than that of 190-bar for the 275- and 230-bar, respectively. This larger area of shear lips might be a reason of the larger impact strength of 275-bars. Moreover, the area of Zone C is apparently also affected by the injection induced PC fibers. The 275-bar showed the thickest sub-skin layer and strongest stress-whitening among these three samples.

More detailed structure information can be obtained from higher magnifications of the fracture surfaces. The slow crack-growth zones (Zone A) of 190-, 230-, 275-bars are shown in Figs. 8(a), 9(a) and 10(a), respectively. The SEM micrograph of the 190-bar (Fig. 8(a)) shows a spherical dispersion of PC phase in PE matrix. Each PC particle is hosted in a slightly larger hole. The matrix ligament surrounding PC particles was severely torn, leaving a lot of dimples or patchwork-like structures on the fracture surfaces. This implies that large plastic deformation and cavitation phenomenon happened in the PE matrix during impact testing. Similar plastic deformation and cavitation was observed in Figs. 9(a) and 10(a) for the 230- and 275-bars. But the PC phase assumed mixed fibrillar and spherical dispersion for 230-bar, and only fibers for 275-bar. The 230- and 275-bars showed smaller micro-void than the 190-bar as a result of finer PC dispersion in the 230- and 270-bars. It is also clear that PC fibers and spherical particles in 230- and 275-bars are smaller those in the 190-bar. This is because during higher temperature molding, PC melt domains suffered further deformation and broke into smaller ones during injection molding. It was observed that zone A for 230-bar is in the intermediate layer, while that for 275-bar is in the sub-skin layer. It is worth noting that the PC fibers also experienced large plastic deformation along with the PE matrix during impact. There are two evidences: (1) some fibers looked very irregular and rough with a long section on the fracture surface, and (2) the deformation of PE matrix in the presence of PC fibrils is larger than that with spherical PC particles, which is obviously the result of the drag along with PC deformation.

The rapid crack-growth zone (zone B) was shown in Figs. 8(b), 9(b) and 10(b), respectively. All three samples displayed PC spherical particles, hence revealing that the observed position is in the core region. The size of the PC dispersed phase showed similar trend as that in the slow crack-growth zone, but the PE matrix experienced different degrees of deformation. For the 190-bar, the matrix ligament underwent less plastic deformation than that in zone A though large holes were seen at which the PC particles were localized. Its fracture surface is rather smooth as a result of brittle fracture. In contrast, the 230- and 275-bars also experienced slightly less plastic deformation than their respective zone A, but a greater amount of PE fibrils were generated, especially for 275-bar.

The crack-blunting zone (zone C) of the bars was shown in Figs. 8(c), 9(c) and 10(c), respectively. As shown in Fig. 8(c), it seemed that the material experienced similar plastic deformation as its slow crack-growth zone. The matrix ligament was plastically torn and surrounded the dispersed PC spherical particles. Apparently, Fig. 8(c) showed the absence of fibrillated structure for both PC phase and matrix PE in the crack-blunting region of the 190-bar. In contrast, dense fibrils were formed in zone C for both molded 230- and 275-bars. And they aligned in the direction perpendicular to the impact loading.

More interesting observation can be found in the SEM micrographs of higher magnifications. The rapid crack-growth zones (zone B, corresponding to the core zone of the bars) are

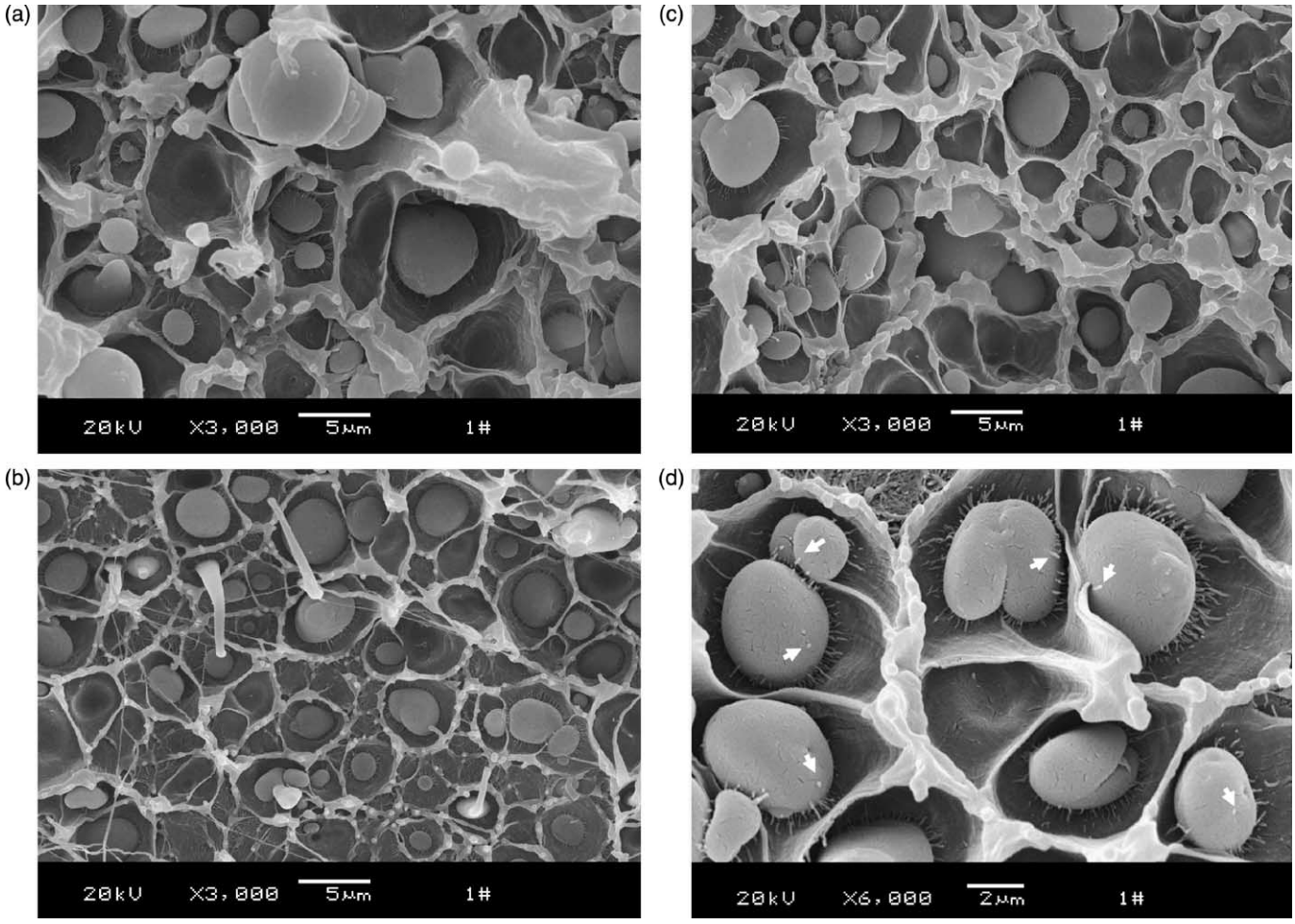

Fig. 8. High magnification SEM micrographs of impact fractured surface of 190-bar. (a) and (d) low crack-growth region; (b) rapid crack-growth region; (c) crack blunting region.

presented in Figs. 8(d)–10(d). There are many filaments around the PC particles (various forms of spherical, ellipsoidal and rodlike) in Fig. 8(d) for B zone of 190-bar, bridging PC domains and PE matrix. There are some protuberant flecks on the surfaces of the PC particles (as designated by the arrows) as a result of broken filaments, indicating strong interfacial adhesion between PC phase and PE matrix. As is known, the solubility parameters of PC and PE are 14.5 and 5.8 $(\mathrm{kJ\ m^{-3}})^{1/2}$, respectively, [43]. The neat PC/PE blend is generally considered to be thermodynamically immiscible and also technologically incompatible due to the large difference of solubility parameters [44]. However, Sue et al. found that the interfacial bonding between the PC and PE is surprisingly strong (as high as 30 MPa) by an unusual operation [45]. They carried out cryogenic ($-160\ ^{\circ}\mathrm{C}$) thin sectioning to study the interfacial bonding between PC and PE. The transmission electronic micrograph clearly showed that the PE particles were still bonded to the PC matrix even after experiencing a dramatic temperature drop from room temperature ($25\ ^{\circ}\mathrm{C}$) down to $-160\ ^{\circ}\mathrm{C}$, and back to room temperature. The thermal stress at the interface corresponding to the maximum temperature excursion was calculated to be as high as $\sim$30 MPa by Boyce's equation [46]. For the interface to be able to withstand such high thermal stress without failure, there must exist a mechanism or mechanisms that allow the two components to interact with each other either physically or chemically, or both. PE lacks functionalities that could react with PC. Sue, et al. suggested that during vigorous mixing, PE chains might have been oxidized to create some reactive sites [45]. This might be true in our case but needs further evidences. Presumably, due to the higher temperature processing, more functional groups should be generated in the 275-bar. However, concurrently, more sever chain session/degradation might also be happened. Their combination may also affect the impact fracture behavior of the blends.

The above microscopic observation may satisfactorily explain the difference in impact toughness for the three samples. The 275-bar showed the highest notch impact energy of 275-bar because it showed (1) the strongest stress whitening (craze formation and cavitation), especially in its fracture initiation zone and ridges of stick–slip line, (2) the most stick–slip lines, (3) the thickest shear lips, (4) the largest crack blunting zone, (5) formation of PE fibrils and (6) plastic deformation of PC fibers. Now the remaining question is that how to explain the toughening mechanism of PC/PE blends injection-molded at different temperatures, which includes

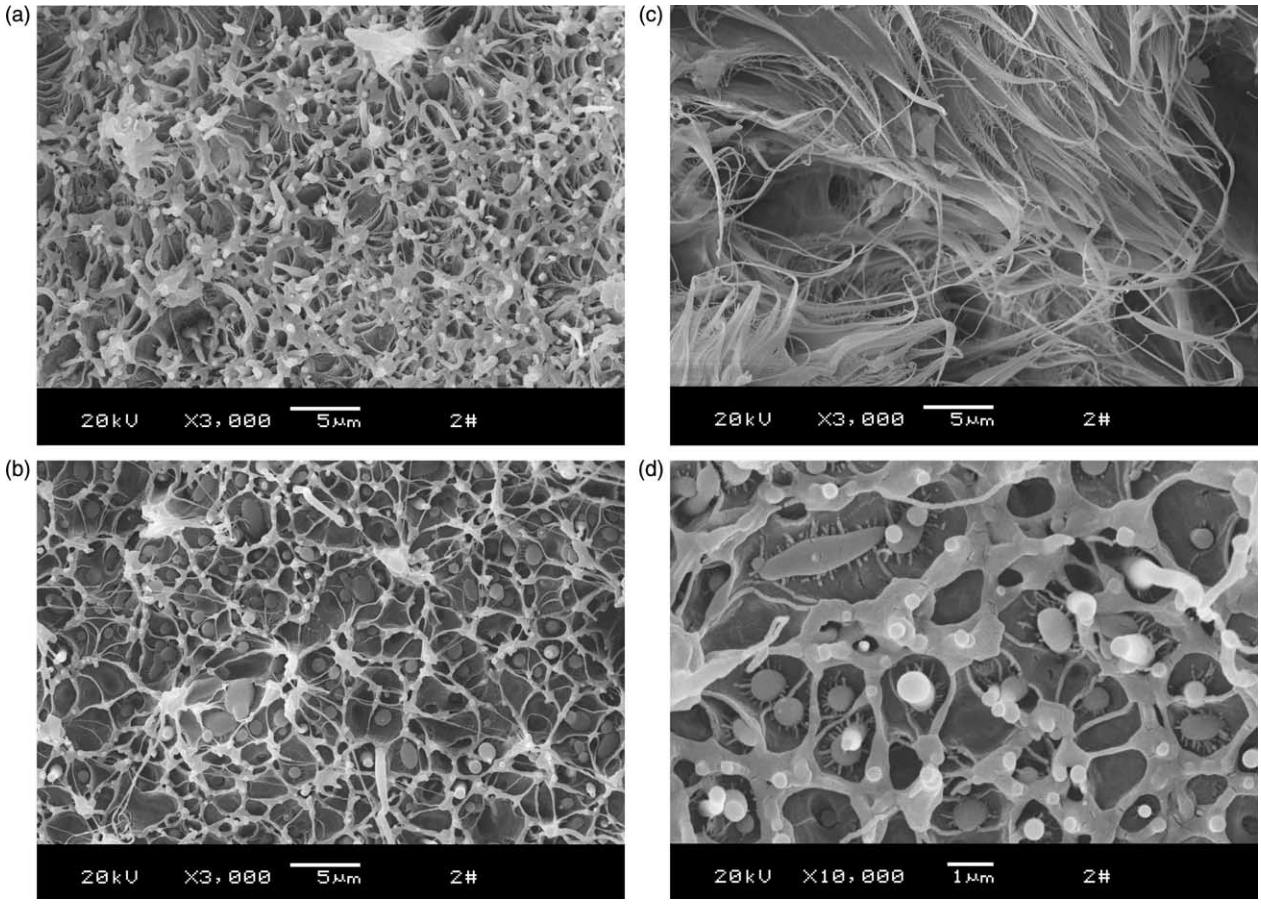

Fig. 9. High magnification SEM micrographs of impact fractured surface of 230-bar. (a) and (d) low crack-growth region; (b) rapid crack-growth region; (c) crack blunting region.

the origin of (1) the difference in overall fracture surfaces, (2) the different PE matrix fibrillation, (3) the influence of PC phase, and (4) the interfacial stress transfer mechanism between PE and PC.

The toughness mechanism, i.e. brittle–ductile transition, has been extensively investigated [47–50]. However, studies of the effect of material morphology, especially PE based blend with a stiffer dispersed phase, on the toughness are limited [42,51, 52]. Kita evaluated the brittle–ductile transition temperature (BDTT) of PEs with different degrees of crystallinity using Charpy impact test [42]. A rise in the crystallinity for high density PE brought about a fall in BDTT and an increase in the Charpy impact value. A crack shielding effect by micro-void formation is proposed as the toughening mechanism for PE. Ravi and Takahashi also investigated the impact fracture behavior of annealed high density PE [41]. Charpy impact test shows that annealing increases the total fracture energy of PE. It is found that as annealing time increases the failure is more ductile with the formation of fibrillar structure. It was proposed that the increased toughness observed in annealed PE is due to the occurrence of micro-voids (or cavities) as the material yields under mode I dynamic tension. The void generation promotes the formation of fibrous structure, which absorbs greater energy than as-received PE.

Essentially, the molding temperatures have similar effect on the morphology and structure of bulk PE as the annealing operation. A higher molding temperature means a longer cooling time and a lower cooling rate, thus, resulting in higher crystallinity and more perfect crystals with larger size as demonstrated in Table 2. Quite possibly, the mechanism proposed by Ravi and Takahashi can partially interpret the toughening in PC/PE blend [41]. Under low strains, the material deforms by the elongation of the amorphous zone between lamellae [53–55]. As the strain increases, the interlamellar separation also increases in higher temperature molded bar [54], and reaches a stage where all the lamellae align themselves nearly normal to the loading direction so that the normal stress on the lamellar surfaces is higher. In the bulk material, the lateral contraction of the deformed amorphous material is constrained by the laterally extended lamellae, and hence the deformation (or interlamellar separation) must be accompanied by cavitation between lamellae, resulting in a large volume change with whitening. The cavitation process must lead to local stress relaxation [42]. The local stress relaxation should have a direct impact on the increase of the fracture energy of the annealed specimens. Additionally, the existence of larger spherulites should enhance the voiding [56]. The dimple-like structure on the surface suggests the formation of micro-voids. The voids help to suppress stress concentration at the crack tip, reducing the near-tip effective stress intensity factor. As the strain increases further, these cavities coalesce to

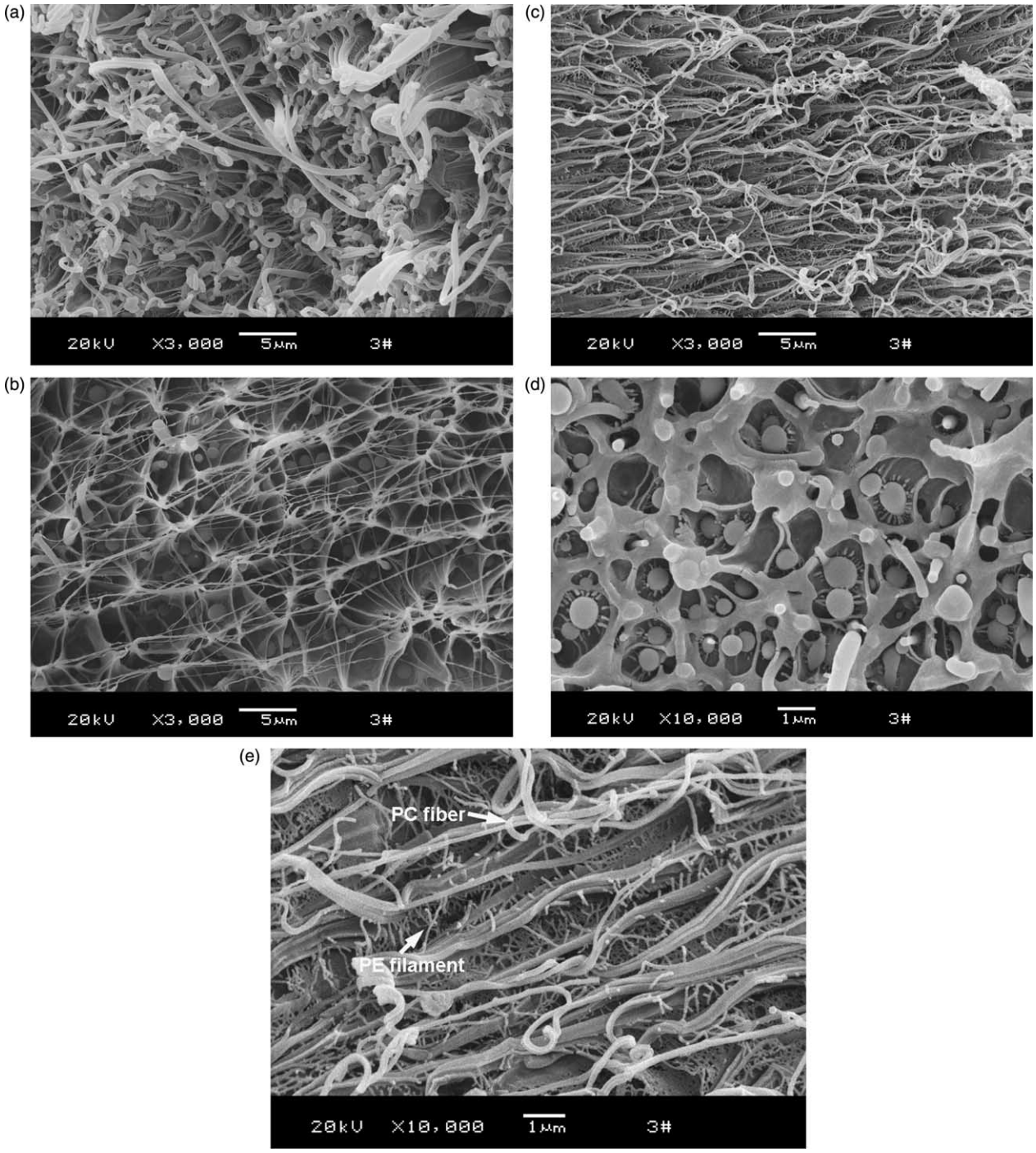

Fig. 10. High magnification SEM micrographs of impact fractured surface of 275-bar. (a) and (d) low crack-growth region; (b) rapid crack-growth region; (c) and (e) crack blunting region.

form elongated voids, resulting in a fibrous structure. SEM micrographs in Figs. 9(c) and 10(b), and especially Fig. 10(c) showed the evidence of such fibrillar structures on the fracture surface. These fibrils behave like miniature samples undergoing micro-necking and sustain larger strain, resulting in higher fracture energy. Thus, the higher crystallinity and more perfect crystals in the 275-bar leads to more considerable cavitation and fibrillar structure of PE matrix.

Regarding the influences of the PC phase with different shapes and size on the impact behavior of PE based blends, the high interfacial contact should be considered. In previous studies [57,58], it was found that high interfacial contact helps to enhance the tensile strength of PE/PC blend by affecting the morphology evolution of PC phase. The high interfacial compressive stress is a result of the thermal history. As the blend is cooled down from processing temperature to room

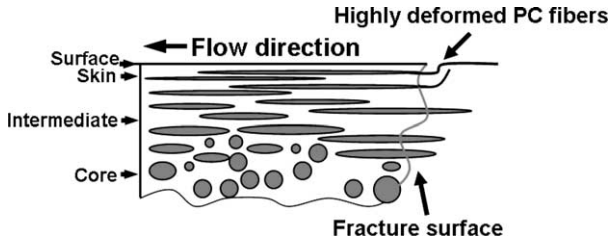

Fig. 11. Schematic representation of impact fractured surface for PEC/PE blend molded at high temperatures (e.g. 230 and 275 °C).

temperature, the matrix PE shrinks more than the dispersed PC phase because of its higher coefficient of thermal expansion coefficient, and additional PE crystallization contraction [57–59]. Consequently, the PE matrix embeds the PC particles tightly and, thus, leads to high compressive stress between the PC dispersed phase and PE matrix. Upon impact fracture, the matrix contracts in the transverse direction, thus, exerting a compressive stress to the PC particles [58]. Therefore, the PC particles received two sorts of compression stresses. With further stretching, due to the relative motion tendency in the interfaces, a frictional force is generated. As a result, the PC particles are under compressive stresses and shear stresses. As the stress between the PC particles and the matrix PE reaches a critical value, the PC fibers will be plastically deformed, and even ruptured upon the additivity of the stress along their length direction as shown in Fig. 11, while the PC spherical particles will not. During such a process, a great amount of energy was dissipated along the PC fibers. This is the so-called fiber formation based toughening (FFBT) mechanism where a remarkable energy absorbing capability results from formation, deformation and fracture of fibers from spherical ones in an incompatible blend [60]. The surfaces of the deformed PC fibers are uneven owing to the non-uniform deformation (Fig. 10(a) and (c)).

Furthermore, the strong interfacial adhesion between PC particles and PE is also in favor of the stress transfer to the surfaces of PC fibers, hence facilitates plastic deformation [60]. As shown in Fig. 10(e), numerous needle-like materials around highly deformed PC fibers are considered to be the broken PE filaments. The strong interfacial bonding leads to the breakage of the PE filaments during impact fracture. The finite element method analysis [61,62] showed that during impact fracture dispersed rubber particles (spheres) in a rubber-toughened blend acted as stress concentrators to cause the three-dimensional stress concentration of matrix ligament around it. The stress concentration occurs not only in the equatorial (90°) but also in the polar (0°) and 45° direction around the dispersed particle. Consequently, the first stress and the equivalent stress become the dominate factors controlling brittle–ductile transition, and reaching their maximum values at the equator region [61,62]. Obviously the elongated PC particles shall cause a strong concentration of stress, especially at the tips in our case. This may accelerate fibrillation of PE matrix and deformation of PC fibers, corresponding to the observation of the SEM fractographs for the 275-bar.

4. Conclusions

The sample injection-molded at 190 °C contained many uniformly dispersed spherical PC particles due to the incapability of flow and deformation of PC phase at this temperature. The samples molded at both 230 and 275 °C showed a typical anisotropic (skin–core) structure, and there were numerous injection-induced PC fibers in the sub-skin layer. The sub-skin layer for the 230-bar is thinner than that of the 275-bar. DSC analysis showed that bars molded at higher temperatures had higher crystallinity and more perfect crystals of PE phase. The three bars molded at different temperatures showed different features during impact fracture. The differences are shown in: (1) overall fracture surface, (2) craze and micro-void formation (stress whitening), (3) fibrillation of PE, and (4) plastic deformation of PC dispersed phase. As the molding temperature increases, the stress whitening becomes stronger, the shear lips become thicker, the amount of the stick–slip lines and the micro-voids increases, and the void becomes smaller. Moreover, upon impact fracturing, numerous fibrils of PE were formed in 230- and 275-bars, and obvious plastic deformation of PC fibers occurred in the 275-bar. All these microscopic features demonstrated that the impact toughness increases with molding temperature. Lamellae texture evolution and high interfacial contact was used to partially interpret the impact fracture behavior. Numerous filaments generated around PC particles on the fracture surfaces, which bridged the PC particles and PE matrix, indicated a high interfacial adhesion between PC particles and PE matrix.

Acknowledgements

The authors gratefully acknowledge the financial support by Program for New Century Excellent Talents in University (NCET) and Sichuan Youth Science and Technology Foundation (Contract Number: 04ZQ026-037).

References

[1] Zhang Z, Yang JL, Friedrich K. Polymer 2004;45:3481–5.
[2] Winter D, Eisenbach CD. Polymer 2004;45:2507–15.
[3] Chapleau N, Mohanraj J, Ajji A, Ward IM. Polymer 2005;46:1956–66.
[4] Karger-Kocsis J, Csikai I. Polym Eng Sci 1987;27:241.
[5] Asami T, Nitta Kh. Polymer 2004;45:5301–6.
[6] Wu S. Polymer 1985;26:1855.
[7] Wu S. Polymer 1990;31:972.
[8] Wu X, Zhu X, Qi ZN. The 8th international conference on deformation, yield and fracture behavior of polymers, Cambridge, UK 1991 p. 78/1.
[9] Fu Q, Wang G. Polym Int 1993;30:309.
[10] Thamm RC. Rubber Chem Technol 1977;50:24.
[11] Favis BD. In: Paul DR, Bucknall CD, editors. Polymer blends volume 1: formulation. New York: Wiley; 2000. p. 502.
[12] Favis BD, Chalifoux JP. Polymer 1988;29:761.
[13] Hsiung CM, Cakmak M, Ulcer Y. Polymer 1996;37:4555.
[14] Evstatiev M, Fakirov S, Krasteva B, Friedrich K, Covas JA, Cunha AM. Polym Eng Sci 2002;42:826.
[15] Fellahi S, Favis BD, Fisa B. Polymer 1996;37:2615.
[16] Fujiyama M. J Appl Polym Sci 1997;63:1015.
[17] Ohlsson B, Tornell B. Polym Eng Sci 1998;38:108.

[18] D'Orazio L, Mancarella C, Martuscelli E, Cecchin G, Corrieri R. Polymer 1999;40:2745.
[19] Ishak ZAM, Chow WS, Ishiaku US, Karger-Kocsis J, Apostolov AA. J Appl Polym Sci 2004;91:175.
[20] Zhang BQ, Zhang J, He JS. J Appl Polym Sci 2004;94:625.
[21] Karger-Kocsis J, Mouzakis DE. Polym Eng Sci 1999;39:1365.
[22] Fu Q, Wang Y, Li QJ, Zhang G. Macromol Mater Eng 2002;287:391.
[23] Wang Y, Zhang Q, Na B, Du RN, Fu Q, Shen KZ. Polymer 2003;44:4261.
[24] Li ZM, Yang W, Yang SY, Huang R, Yang MB. J Mater Sci 2004;39:413.
[25] Li ZM, Xie BH, Yang SY, Huang R, Yang MB. J Mater Sci 2004;39:433.
[26] Li ZM, Huang CG, Yang W, Yang MB, Huang R. Macromol Mater Eng 2004;289:1004.
[27] Liu TM, Baker WE. Polym Eng Sci 1992;32:944.
[28] Friedrich K, Ueda E, Kamo H, Evstatiev M, Krasteva B, Fakirov S. J Mater Sci 2002;37:4299.
[29] Na B, Wang Y, Du RN, Fu Q, Men YF. J Polym Sci, Part B: Polym Phys 2004;42:1831.
[30] Li ZM, Yang W, Li LB, Xie BH, Huang R, Yang MB. J Polym Sci, Part B: Polym Phys 2004;42:374.
[31] Li ZM, Li LB, Shen KZ, Yang MB, Huang R. Polymer 2005;46:5358–67.
[32] Odell JA, Grubb DT, Keller A. Polymer 1978;19:617.
[33] Southern JH, Porter RS. J Appl Polym Sci 1970;14:2305.
[34] Yamazaki S, Watanabe K, Okada K, Yamada K, Tagashira K, Toda A, et al. Polymer 2005;46:1685–92.
[35] Somani RH, Hsiao S, Yang L. Macromolecules 2002;35:9096.
[36] Nowacki R, Monasse B, Piorkowska E, Galeski A, Haudin JM. Polymer 2004;45:4877–92.
[37] Mendoza R, Regnier G, Seiler W, Lebrun JL. Polymer 2003;44:3363–73.
[38] Kubat J, Mason JA. Polym Eng Sci 1983;23:869.
[39] Victor T, Musa R. J Appl Polym Sci 1978;22:2341.
[40] Baker AME, Windle AH. Polymer 2001;42:667.
[41] Raw S, Takahashi K. Polym Eng Sci 2002;42:2146.
[42] Kitao K. Polym Eng Sci 1997;37:777.
[43] Wunderlich B. Macromolecular physics. New York: Academic Press; 1973.
[44] Kunori T, Geil PH. J Macromol Sci Phys 1980;B18:93.
[45] Sue HJ, Huang J, Yee AF. Polymer 1992;33:4868.
[46] Boyce ME, Argon AS, Parks DM. Polymer 1987;28:1681.
[47] Zewi IG, Rudik WJ, Corneliussen RD, Lind EV. Polym Eng Sci 1980; 20:622.
[48] Mandell JF, Roberts DR, McGarry FJ. Polym Eng Sci 1983;23:404.
[49] Brown N, Ward IM. J Mater Sci 1983;18:1405.
[50] Fleissner M. Angew Makromol Chem 1982;103:167.
[51] Tjong SC, Xu SA. J Appl Polym Sci 1998;68:1099.
[52] Bai SL, Wang GT, Hiver JM, G'Sell C. Polymer 2004;45:3063–71.
[53] Butler MF, Donald AM, Ryan AJ. Polymer 1997;38:5521.
[54] Adams WW, Yang D, Thomas EL. J Mater Sci 1986;21:2239.
[55] Brady JM, Thomas EL. J Mater Sci 1989;24:3311.
[56] Channell AD, Clutton EQ, Capaccio G. Polymer 1994;35:3893.
[57] Leclair A, Favis BD. Polymer 1996;37:4723.
[58] Li ZM, Fu XR, Yang SY, Yang MB, Yang W, Huang R. Polym Eng Sci 2004;44:1561.
[59] Fisa B, Favis BD, Bourgeois S. Polym Eng Sci 1990;30:1051.
[60] Li ZM, Yang MB, Feng JM, Huang R. J Mater Sci 2001;36:2013.
[61] Eshelby JD. Proc R Soc 1957;A241:376.
[62] Zhang R, Lu S. Appl Compos Mater 1994;1:115.